Journal of Global Change Data & Discovery. 2018, 2(2): 184-189
DOI:10.3974/geodp.2018.02.10
www.geodoi.ac.cn

Comprehensive Electromagnetic Experimental Dataset in Deep Mineralization Mechanism in Wuxi Polymetallic Ore Deposit of Anhui Province, China

Lin, F. L.[1] Wang, G. J.[2*] Yang, X. Y.[3]

1. Key Discipline of Electronic Science and Technology of Henan Province, School of Electronics and Electrical Engineering, Henan Normal University, Xinxiang 453007, China;
2. Institute of Geology and Geophysics, Chinese Academy of Sciences, Beijing 100029, China;
3. School of Earth and Space Science, University of Science and Technology of China, Hefei 230026, China

Abstract: The Wuxi polymetallic ore deposit lies between the middle and lower reaches of the Yangtze River polymetallic metallogenic belt and South China metallogenic belt. To study the deep metallogenic mechanism, a comprehensive electromagnetic prospecting of the area was conducted during the periods of March–November 2011 and October–November 2012. During the initial inspection, the main types of rock exposed in the area were collected, and the physical properties of the rocks were measured in the laboratory. Three different electromagnetic methods were applied in the integrated exploration: the high-precision ground magnetic method, dual-frequency induced polarization method, and controlled source audio magnetotelluric method (CSAMT). The dataset was consisted of two parts. Part 1: raw data collected in situ survey and analysis in the laboratory, including (1) The physical property data of the main rock types exposed in Wuxi polymetallic ore deposit; (2) GPS data of lines and points in situ survey; (3) Raw data and corrected data got in ground precise magnetic survey; (4) Plane amplitude frequency and apparent resistivity data using dual frequency induced polarization method; and (5) CSAMT fieldwork log and raw data in Jingxian, Wuxi, China. Part 2: Split data, including (1) Split results of corrected data using the ground high-precision magnetic survey; (2) Split results of amplitude frequency using the dual frequency induced polarization method; (3) Split results of the deep survey line apparent resistivity using CSAMT method. Different methods of collecting data obtained through the split process can reach 25 m × 25 m × 25 m spatial resolution. The dataset was archived in .xlsx, .grd, .cmd, .cms, .cmv, .csv, .cmr, .csr, and .pdf formats with the data size of 31.4 MB (compressed into one file, 6.86 MB).

Keywords: comprehensive electromagnetic; Wuxi polymetallic ore; CSAMT; dual frequency induced polarization method; high-precision ground magnetic method

Received: 04-02-2018; **Accepted:** 22-06-2018; **Published:** 25-06-2018

Foundation(s): Ministry of Science and Technology of P. R. China (2016YFC0600507); Henan Normal University doctoral research fund (5101239170002); NSFC-Henan United Fund (U704134).

***Corresponding Author:** Wang, G. J. C-4555-2018, Institute of Geology and Geophysics, Chinese Academy of Sciences, gjwang@mail.iggcas.ac.cn

Data Citation: [1] Lin, F. L., Wang, G. J., Yang, X. Y. Comprehensive electromagnetic dataset in deep mineralization mechanism in Wuxi polymetallic ore deposit of Anhui province, China [J]. *Journal of Global Change Data & Discovery*, 2018, 2(2): 184–189. DOI: 10.3974/geodp.2018.02.10.

[2] Lin, F. L., Wang, G. J., Yang, X. Y. Comprehensive electromagnetic experimental dataset in deep mineralization mechanism in Wuxi polymetallic ore deposit of Anhui province, China [DB/OL]. Global Change Research Data Publishing & Repository, 2018. DOI: 10.3974/geodb.2018.03.08.V1.

1 Introduction

The Wuxi polymetallic ore deposit, located between the middle and lower reaches of the Yangtze River polymetallic metallogenic belt and South China metallogenic belt, is a new prospecting area in the Jiangnan orogan. The analysis of the characteristics of the deep electromagnetic characteristics of this area is of great significance for the study of the deep mineralization mechanism operating in the Wuxi mining area. At the same time, if it could be confirmed that the Wuxi mining area is a porphyry deposit, the similarity of the metallogenic belt formed by the South China metallogenic belt and subduction could be confirmed, which would promote the study of metallogenic geology in the entire South China region[1–3].

2 Metadata of Dataset

The metadata that comprises the comprehensive electromagnetic experimental dataset in deep mineralization mechanism in Wuxi polymetallic ore deposit of Anhui province, China[4] is summarized in Table 1. It includes full name, short name, authors, and year that the dataset was compiled, data format, data size, data files, data publisher, data sharing policy, etc.

Table 1 Metadata summary of the comprehensive electromagnetic experimental dataset in deep mineralization mechanism in Wuxi polymetallic ore deposit of Anhui province, China

Items	Description
Dataset full name	Comprehensive electromagnetic experimental dataset in deep mineralization mechanism in Wuxi polymetallic ore deposit of Anhui province, China
Dataset short name	ComprehElectromagneticDataPolymetallicOreWuxi
Authors	Lin, F. L. M-5558-2018, Henan Normal University, linfangli@htu.edu.cn Wang, G. J. C-4555-2018, Institute of Geology and Geophysics, Chinese Academy of Sciences, gjwang@mail.iggcas.ac.cn Yang, X. Y. M-5549-2018, University of Science and Technology of China, xyyang555@163.com
Geographical region	Wuxi village, Jingxian county, Hefei city, Anhui province
Year	2011–2015
Data format	.xls, .grd, .cmd, .cms, .cmr, .csv, .csr, .pdf
Data size	6.86 MB (after compression)
Data files	The comprehensive electromagnetic dataset of the Wuxi polymetallic ore deposit in southern Anhui included two parts. Part 1: data obtained from field measurements and laboratory analysis, including (1) rock property measurement data; (2) field-measured line-to-point GPS data; (3) the original magnetic field data and the corrected magnetic field data obtained by ground high-precision magnetic measurement; (4) plane amplitude frequency and apparent resistivity data obtained by the dual frequency polarization method; and (5) CSAMT, i.e., field work newspaper and raw data collected daily. Part 2: split data, including (1) split results of the corrected magnetic field obtained by high-precision ground magnetic measurement; (2) split results of amplitude frequency obtained by the dual-frequency polarization method; and (3) split results of each survey line's deep apparent resistivity obtained by the CSAMT method
Foundation(s)	Ministry of Science and Technology of P. R. China (2016YFC0600507); Henan Normal University doctoral research fund (5101239170002); NSFC-Henan United Fund (U704134)
Data publisher	Global Change Research Data Publishing & Repository, http://www.geodoi.ac.cn
Address	No. 11A, Datun Road, Chaoyang District, Beijing 100101, China

(***To be continued on the next page***)

(***Continued***)

Items	Description
Data sharing policy	***Data*** from the Global Change Research Data Publishing & Repository includes metadata, datasets (data products), and publications (in this case, in the *Journal of Global Change Data & Discovery*). The ***Data*** sharing policy is as follows. (1) ***Data*** are openly available and can be freely downloaded via the Internet; (2) End users are encouraged to use ***Data*** subject to citation. (3) Users, who are by definition also value-added service providers, are welcome to redistribute ***Data*** subject to written permission from the GCdataPR Editorial Office and the issuance of a ***Data*** redistribution license. (4) If ***Data*** are used to compile new datasets, the '10% principal' should be followed such that any ***Data*** records utilized should not surpass 10% of the new dataset contents, while sources should be clearly noted in suitable places in the new dataset[5]

3 Methods

All the data used in this study were collected in the field and subjected to real-time electromagnetic interference. The main goal 33 of the data processing was to remove all electromagnetic interferences, thereby extracting magnetic anomalies, induced anomalies, and resistivity anomalies caused by underground mineral resources.

3.1 Algorithm Principle

3.1.1 Principle of the Ground High-precision Magnetic Algorithm

The proton magnetometer was used in this study to measure the absolute magnetic field strength. This is necessary to eliminate the influence of the earth's magnetic field caused by the movement of the earth's shape and rotation in order to obtain the true difference in the geomagnetic field between each station. Therefore, corrections, including a normal gradient correction, height correction, and geomagnetic day-to-day correction, need to be made.

When the normal gradient correction is performed, the geomagnetic T_0 value of the 1 km×1 km node in the survey area can be calculated by using the Gaussian coefficient provided by the IGRF1990.0 model of the international geomagnetic reference field.

$$T_0 = \sqrt{X^2 + Y^2 + Z^2} = \sqrt{H^2 + Z^2} \quad (1) \qquad \frac{\partial T_0}{\partial X} = \frac{3ZH}{2RT_0} \quad (2)$$

Where *X*, *Y*, *H*, and *Z* are the east, north, horizontal, and vertical components of the geomagnetic field, respectively. *R* is the average radius of the earth (6,371 km). By passing the isobar of the total base point to the zero line, there is a 1 nT reduction for each contour line northward.

Magnetic field along the vertical magnetic field gradient: $$\frac{\partial T_0}{\partial R} = -\frac{3T_0}{R} \quad (3)$$

when T_0 = 50,000 nT, the vertical gradient of the magnetic field is −0.024 nT/m. Therefore, the height correction is based on the vertical gradient of the geomagnetic field and is corrected based on the elevation of each measurement point.

Spatial magnetic field disturbances include rapid vibrations ranging from 0.2 to 1,000 s, with typical amplitudes of 0.01 to 5 nT (sometimes 10 to 20 nT). The high-precision magnetic measurement need to correct this periodic variation of the geomagnetic field, and remove the influence of changes in the earth's own magnetic field on the observed magnetic field through the daily change correction, and therefore there is a requirement for the observation of daily changes.

For the result interpretation, supplementary measurements were made based on previous ground high-precision magnetic measurements. To ensure the consistency of the two results, repeated measurements of some measurement points were used to normalize the two results.

$$\Delta V = \frac{\sum_{i=1}^{n}(V_{1i} - V_{2i})}{n} \tag{4}$$

$$V_{2i} = V_{1i} - \Delta V \tag{5}$$

Where V_{1i} and V_{2i} are the magnetic field data of the first and second measurements, respectively, and the normalized parameter ΔV is calculated by repeating the measurement data.

3.1.2 Principle of the Dual-frequency Induction Algorithm

The dual frequency induced polarization (DFIP) method was used to superimpose the square wave signals of two frequencies to form a dual-frequency combined signal. The dual-frequency signal was transmitted, and then the potential difference information for the total field due to the underground excitation containing the two main frequencies was simultaneously received[6]. Therefore, the potential difference between the low and high frequencies could be obtained once, and the apparent amplitude frequency F_s was calculated:

$$F_s(\%) = \frac{\Delta V(f_L) - \Delta V(f_H)}{\Delta V(f_L)} \times 100\% \tag{6}$$

Where $\Delta V(f_L)$ and $\Delta V(f_H)$ are low frequency and high frequency potential differences, respectively.

3.1.3 Principle of the Controlled Source Audio Magnetotelluric Algorithm

The CSAMT inversion calculation is based on the theory of electromagnetic wave propagation and the electric and magnetic field formula of the horizontal electric dipole source derived from Maxwell's equations on the ground:

$$E_x = \frac{I \cdot AB \cdot \rho_1}{2\pi r^3} \cdot (3\cos^2\theta - 2) \tag{7}$$

$$E_y = \frac{3 \cdot I \cdot AB \cdot \rho_1}{4\pi r^3} \cdot \sin 2\theta \tag{8}$$

$$E_z = (i-1)\frac{I \cdot AB \cdot \rho_1}{2\pi r^2} \cdot \sqrt{\frac{\mu_0 \omega}{2\rho_1}} \cdot \cos\theta \tag{9}$$

$$H_x = -(1+i)\frac{3I \cdot AB}{4\pi r^3} \cdot \sqrt{\frac{2\rho_1}{\mu_0 \omega}} \cdot \cos\theta \cdot \sin\theta \tag{10}$$

$$H_y = (1+i)\frac{I \cdot AB}{4\pi r^3} \cdot \sqrt{\frac{2\rho_1}{\mu_0 \omega}} \cdot (3\cos^2\theta - 2) \tag{11}$$

$$\rho_s = \frac{1}{5f}\frac{|E_x|^2}{|H_y|^2} \tag{12}$$

where I is the transmitted current; AB is the length of the transmission dipole; and r is the transmission and reception distance.

The electric field in the x direction, E_x, is divided by the magnetic field in the y direction, H_y, to obtain an underground apparent resistivity formula by simplifying Equation (12).

(1) Terrain Correction

Due to the large slope of the survey line, the slope distance between the points was very different from the horizontal distance (25 m) between the two pre-designed points. It is well known that the Cagniard apparent resistivity is calculated from perpendicular horizontal magnetic fields and electric field. It is proportional to the square of E_x and inversely propor-

tional to the square of H_y. When working in mountainous terrain, H_y is horizontal magnetic field because the magnetic probe is placed along the contour line. However, the electric field E_x which is measured along the slope direction is no longer a horizontal electric field. Therefore, H_y is close to the real situation, and E_x contains a certain error. As a result, there is also a certain error in the apparent resistivity value which should be corrected. The commercial processing software calculates the electric field using the formula $E_x = \Delta V/\Delta x$, where ΔV is the potential difference between the two electrodes and Δx is the horizontal distance between the two electrodes. The measured electric field is $\Delta V_{slope}/\Delta x$. Therefore, the horizontal electric field should be corrected to:

$$Ex=\Delta V_{slope}\, cos\theta/\Delta x \tag{13}$$

where θ is the slope angle.

(2) Static Correction

The formula used to calculate the Cagniard apparent resistivity was derived for the far zone (or wave zone). In the transition zone or near zone, the Cagniard apparent resistivity will be distorted. Due to the near-field effect of the CSAMT method, the penetration depth of the signal does not always increase as the frequency decreases. When there is a local conductive unevenness near the surface, current through the surface of the uneven body form an "accumulated charge", thereby generating an additional electric field proportional to the external current field.

(3) Electromagnetic Interference Rejection

Because some of the data collected were subject to relatively severe electromagnetic interference, we performed an electromagnetic interference removal process on the original data before performing the inversion calculation.

3.2 Flowchart of Data Processing

According to the basic principles of the three methods, the collected data is processed accordingly. Flowchart of data processing is shown in Figure 1.

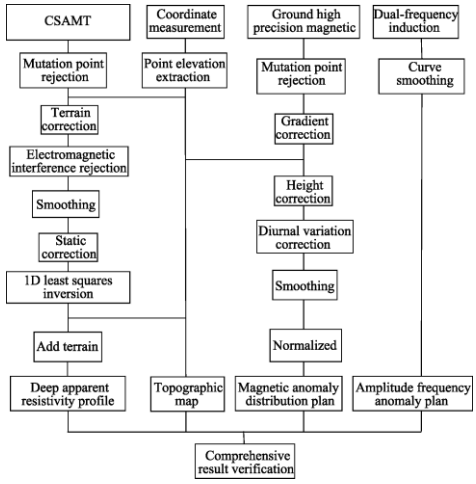

Figure 1 Flowchart of data processing

4 Results and Validation

4.1 Data Products

On the basis of the dataset, the coordinates and elevation data of each point in the Wuxi mining area, plane magnetic anomaly distribution, abnormal distribution of the plane amplitude frequency, and depth apparent resistivity anomaly data could be obtained by calculation (Table 2)[7].

4.2 Validation

Compared with a borehole geological map, the resistivity distribution characteristics were found to be basically consistent with the lithology distribution in the area. The drilling results further proved that surface mineralization in the area was not obvious, the overall resistivity was high, and the rock mass was characterized by a high resistance relative to other

rocks. The mineralization could significantly reduce the resistivity of the rock formation.

Table 2 The slice resistivity anomalies at different depths (excerpt)

Number	File name	Data description
1	line5000	Deep resistivity data of line 5000, the x-axis is the point number and the y-axis is the depth
2	line5200	Deep resistivity data of line 5200, the x-axis is the point number and the y-axis is the depth
3	line5400	Deep resistivity data of line 5400, the x-axis is the point number and the y-axis is the depth
4	line5600	Deep resistivity data of line 5600, the x-axis is the point number and the y-axis is the depth
5	line5800	Deep resistivity data of line 5800, the x-axis is the point number and the y-axis is the depth
6	line6000	Deep resistivity data of line 6000, the x-axis is the point number and the y-axis is the depth
7	line6200	Deep resistivity data of line 6200, the x-axis is the point number and the y-axis is the depth
8	line6400	Deep resistivity data of line 6400, the x-axis is the point number and the y-axis is the depth
9	line7000	Deep resistivity data of line 7000, the x-axis is the point number and the y-axis is the depth
10	line7200	Deep resistivity data of line 7200, the x-axis is the point number and the y-axis is the depth
11	line7400	Deep resistivity data of line 7400, the x-axis is the point number and the y-axis is the depth
12	line7600	Deep resistivity data of line 7600, the x-axis is the point number and the y-axis is the depth
13	line7800	Deep resistivity data of line 7800, the x-axis is the point number and the y-axis is the depth
14	line8000	Deep resistivity data of line 8000, the x-axis is the point number and the y-axis is the depth

5 Discussion and Conclusion

According to the polarization rate and the scale of the low-resistance body, the Wuxi mining area is a favorable porphyry copper (molybdenum gold) metallogenic prospecting area. This further expands the possible range of formation of porphyry copper deposits due to subduction in the South China metallogenic belt, and will inform regional metallogenic geological research in South China. The dataset is based on four databases: high-precision coordinates, ground high-precision magnetic measurements, dual-frequency excitation, and CSAMT data collected in the Wuxi mining area.

Author Contributions

Wang, G. J. and Yang, X. Y. designed the algorithms of the dataset; Lin, F. L. contributed to the data processing and analysis; and Lin, F. L. wrote the data paper.

References

[1] Sun, W. D., Ling, M. X., Yang, X. Y., *et al*. Ridge subduction and porphyry copper-gold mineralization: an overview [J]. *Science in China Series D*: *Earth Sciences*, 2010, 53(4): 475–484.

[2] Sun, W. D., Liang, H. Y., Ling, M. X., *et al.* The link between reduced porphyry copper deposits and oxidized magmas [J]. *Geochimica et Cosmochimica Acta*, 2013, 103: 263–275.

[3] Li, S., Sun, S. J., Yang, X. Y., *et al*. Petrological geochemistry and chronology of ore-bearing intrusion in Wuxi porphyry gold deposit, in South Anhui province [J]. *Geotectonica et Metallogenia*, 2015, 39(1): 153–166.

[4] Lin, F. L., Wang, G. J., Yang, X. Y. Comprehensive electromagnetic experimental dataset in deep mineralization mechanism in Wuxi polymetallic ore deposit of Anhui province, China [DB/OL]. Global Change Research Data Publishing & Repository, 2018. DOI: 10.3974/geodb.2018.03.08.V1.

[5] GCdataPR Editorial Office. GCdataPR data sharing policy [OL]. DOI: 10.3974/dp.policy.2014.05 (Updated 2017).

[6] He, J. S. Dual-frequency IP Method [M]. Beijing: Higher Education Press, 2006.

[7] Lin, F. L., Wang, G. J., Yang, X. Y. Application of comprehensive electromagnetic study in deep mineralization mechanism—a case study of the Wuxi polymetallic ore deposit, south Anhui [J]. *Chinese Journal of Geophysics*, 2016, 59(11): 4323–4337, DOI: 10.6038/cjg20161132.